--- --- --- --- --- --- --- --- ---

Lead isotope variations across terrane boundaries of the Tien Shan and Chinese Altay

--- --- --- --- --- --- --- --- ---

Chiaradia, Massimo; Konopelko, Dmitry; Seltmann, Reimar; Cliff, Robert A.

ARTICLE

Massimo Chiaradia · Dmitry Konopelko ·
Reimar Seltmann · Robert A. Cliff

Lead isotope variations across terrane boundaries of the Tien Shan and Chinese Altay

Abstract The Altaid orogen was formed by aggregation of Paleozoic subduction–accretion complexes and Precambrian basement blocks between the Late Proterozoic and the Early Mesozoic. Because the Altaids are the site of abundant granitic plutonism and host some of the largest gold deposits in the world, understanding their formation has important implications on the comprehension of Phanerozoic crustal growth and metallogeny. In this study, we present the first extensive lead isotope data on magmatic and metasedimentary rocks as well as ore deposits of the southern part of the Altaids, including the Tien Shan (Tianshan) and southern Altay (Altai) orogenic belts. Our results show that each terrane investigated within the Tien Shan and southern Altay is characterized by a distinct Pb isotope signature and that there is a SW–NE Pb isotope gradient suggesting a progressive transition from a continental crust environment in the West (the Kyzylkum and Kokshaal segments of the Southern Tien Shan) to an almost 100% juvenile (MORB-type mantle-derived) crust environment in the East (Altay). The Pb isotope signatures of the studied ore deposits follow closely those of magmatic and metasedimentary rocks of the host terranes, thus supporting the validity of lead isotopes to discriminate terranes. Whereas this apparently suggests that no unique reservoir has been responsible for the huge gold concentration in this region, masking of a preferential Pb-poor Au-bearing reservoir by mixing with Pb-rich crustal reservoirs during the mineralizing events cannot be excluded.

Keywords Tien Shan · Altay · Lead isotopes ·
Ore deposits · Magmatic rocks

M. Chiaradia · R. A. Cliff
School of Earth and Environment, University of Leeds,
Leeds LS2 9JT, UK

D. Konopelko
Geological Faculty, St. Petersburg State University,
7/9 University Embankment,
St. Petersburg 199034, Russia

R. Seltmann
Natural History Museum, Department of Mineralogy,
CERCAMS,
London SW7 5BD, UK

Present address:
M. Chiaradia (✉)
Department of Mineralogy, University of Geneva,
Rue des Maraîchers 13,
Geneva 1205, Switzerland
e-mail: Massimo.Chiaradia@terre.unige.ch
Tel.: +41-22-3796634
Fax: +41-22-3793210

Introduction

The giant Altaid orogenic collage, also called the Central Asian Orogenic Belt (CAOB; Jahn et al. 2000), consists of Paleozoic subduction–accretion complexes and magmatic arcs, as well as Precambrian micro-continents, which were accreted, consolidated, and deformed during Late Proterozoic and Paleozoic collisional events and subsequent Alpine-Himalayan deformations (e.g., Sengör et al. 1993; Sengör and Natal'in 1996). This "Turkic-type" orogenic collage, formed by accretion (e.g., Sengör and Natal'in 1996), differs markedly from the Himalayan and Alpine orogens, formed by frontal collision of two continents. It is also a site of abundant syn- and post-collisional magmatism, and hosts some of the largest gold deposits in the world (Drew et al. 1996; Rui et al. 2002; Yakubchuk et al. 2002; Liu et al. 2003). Therefore, knowledge of the processes of formation of the Altaids has important implications on the understanding of Phanerozoic crustal growth and metallogeny.

Radiogenic isotopes are able to constrain the terrestrial reservoirs that provide the materials that make up orogens and mineralization and, therefore, to characterize the crust and metallogenic evolution of orogenic belts (e.g., Macfarlane et al. 1990; Chiaradia et al. 2004). Previous studies have essentially used neodymium isotope systematics, recording positive ε_{Nd} values and young Nd model ages in granitic rocks of the Altay, Junggar, and Central

Kazakhstan (Han et al. 1997; Chen et al. 2000a; Heinhorst et al. 2000; Jahn et al. 2000; Hong et al. 2003) that have led to estimates of a 70 to 100% juvenile (mantle) component in these rocks (Jahn et al. 2000). In contrast, only scattered lead isotope data are available for some ore deposits but not for rocks of the southern Altaids (Li et al. 1998; Wang et al. 2002). Lead isotopes would be a precious addition to the isotope systematics of the Altaids because, due to the large Pb concentration differences between mantle (0.03 ppm) and crustal (23.1 ppm) reservoirs (e.g., Zartman and Haines 1988), they allow the tracing of minimal crustal contamination of mantle-derived magmas and therefore permit to test the model of juvenile crustal growth based on the Nd data. Additionally, lead isotopes can be measured on ore minerals, which are precipitated by hydrothermal fluids after more or less extensive interaction with country rocks, and, as such, provide further information on the nature of the crustal substratum.

In this study, we present more than 100 new Pb isotope data on magmatic and metasedimentary rocks as well as ore deposits of the southern part of the Altaids, including the Tien Shan and southern Altay orogenic belts. Our data cover an approximately SW–NE transect, about 2,000 km long and 300 km wide, from the Kyzylkum desert of Uzbekistan in the west to the Chinese Altay of Xinjiang in the east (Fig. 1). The aims of this study are to (1) provide the first large-scale lead isotope dataset on crustal materials (magmatic and metasedimentary rocks, ore deposits) of the southern Altaids, (2) check for Pb isotope variations among different terranes forming the southern part of the Altaid orogenic collage, and (3) infer the metal sources in the gold deposits to establish whether a preferential reservoir has been responsible for the gold enrichment of this region.

Fig. 1 Geotectonic map of Central Asia (modified from Yakubchuk et al. 2003). The *rectangle* represents the investigated area within the southern Altaids (Fig. 2)

Geological setting

The Altaids

The Altaid orogenic collage includes several orogenic belts (the Mongol-Okhotsk, Altay-Sayan, Kazakhstan, Tien Shan, and Urals) situated east of the East European craton, surrounding the Siberian craton from west, south, and east, and bordered by the Alay-Tarim and Karakum micro-continents in the south (Sengör et al. 1993; Fig. 1). Much of the Altaid orogenic collage was formed by the accretion of allochthonous fragments, including subduction–accretion complexes, island arcs, ophiolites, and micro-continents, between the Late Proterozoic and the Early Mesozoic (Mukhin et al. 1989; Zonenshain et al. 1990; Allen et al. 1992; Sengör et al. 1993; Allen et al. 1995; Sengör and Natal'in 1996). Sengör et al. (1993) viewed the various fold-and-thrust belts of the southern Altaids as formed along a single subduction zone. In their interpretation, all Precambrian fragments, now found in the Altaids, were detached from the joint Eastern Europe and Siberian cratons in the Late Proterozoic, opening up the Khanty-Mansi basin, whereas subduction in front of them produced the Kipchak arc built on Precambrian basement. Giant accretion–subduction complexes have formed since the Early Paleozoic and were accreted against the Kipchak arc together with island arcs, ophiolitic complexes, and micro-continents. Subsequently, they were sliced by large-scale strike-slip faults, and oroclinally bent due to the clockwise rotation of Siberia relative to Eastern Europe, which caused the progressive closing-up of the Khanti-Mansi basin during the Caledonian (approximately 420 Ma) and Hercynian (approximately 280 Ma) collisional events. The Paleo-Turkestan ocean existing to the south of the newly formed Caledonian paleocontinents (e.g., Kazakhstan, Altay) was closed as a result of the Hercynian collision with the Alay-Tarim and Karakum micro-continents and final assemblage of the southern Altaids.

This general interpretation has been shared by later investigations (e.g., Jahn et al. 2000; Yakubchuk et al. 2002; Xiao et al. 2004; Yakubchuk 2004), although with some variations, namely, the existence of three Proterozoic–Early Paleozoic arcs (Kipchak, Tuva-Mongol, Mugodzhar-Rudny Altai) instead of the Kipchak arc alone, the enhanced role of ophiolites, and the importance of the accretion of micro-continents. Further details on the evolution of the Altaid orogenic collage can be found in the studies mentioned above. Below, we describe the orogenic belts of the Tien Shan and Chinese Altay investigated in this study (Figs. 1 and 2).

The Tien Shan

The Hercynian Tien Shan orogen was formed during the Late Paleozoic (Hercynian) collision between the Karakum and Alay-Tarim micro-continents and the Paleo-Kazakhstan continent, a Caledonian component of the Altaid Collage. The Tien Shan is composed of three major
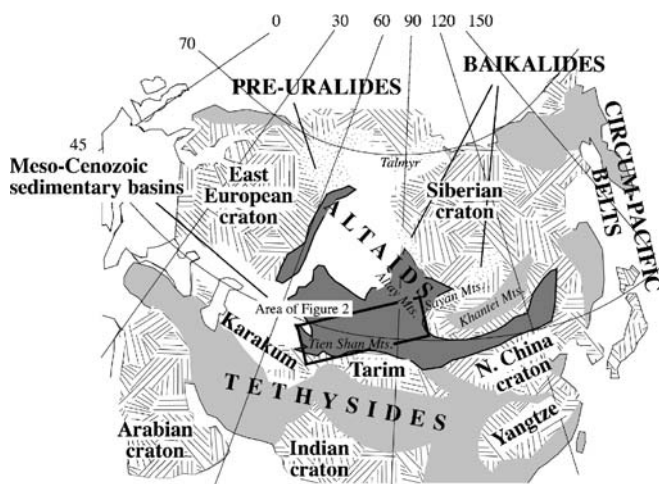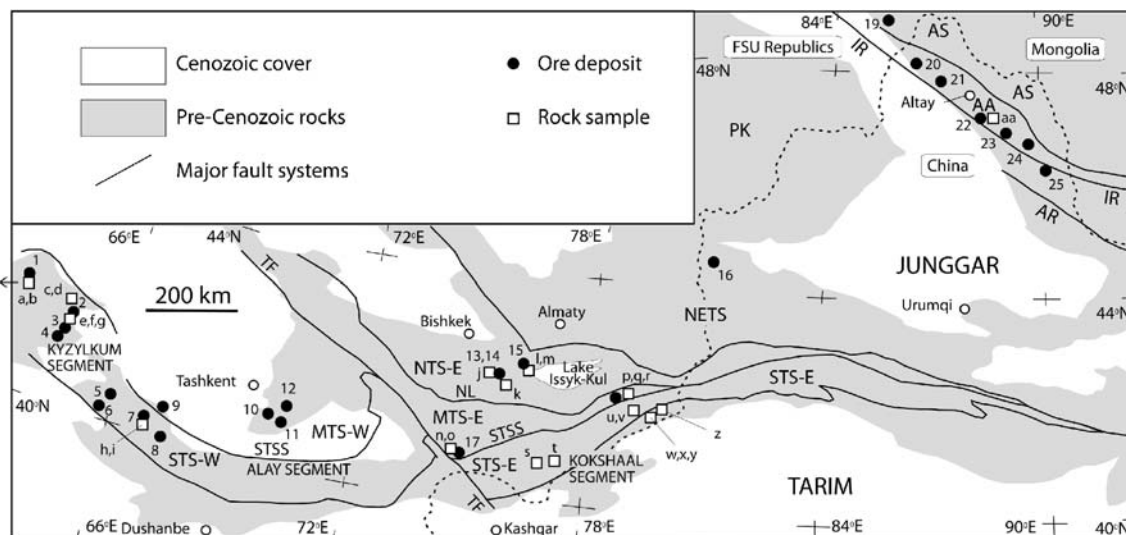
Fig. 2 Principal terranes and tectonic lineaments of the Tien Shan and Chinese Altay and sampling sites. The numbers and letters identifying the mineral deposit and rock sampling sites, respectively, correspond to those reported in Tables 1 and 2. Ore deposits: *1*=Sarytau; *2*=Muruntau; *3*=Amantaitau; *4*=Daugyztau; *5*=Guzhumsay; *6*=Sarmich; *7*=Zarmitan; *8*=Mardjanbulak; *9*=Uchkulach; *10*=Kalmakyr; *11*=Kochbulak; *12*=Ustarasay; *13*=Boordu; *14*=Taldybulak Levoberezhny; *15*=Aktyuz; *16*=Axi; *17*=Makmal; *18*=Kumtor; *19*=Manka; *20*=Ashele; *21*=Saidu; *22*=Shangkelan; *23*=Mengku; *24*=Keketale; *25*=Kalatonge. Rock samples: *a,b*=Sarytau; *c,d*=Muruntau; *e,f,g*=Muruntau-Tamdy; *h,*

i=Koshrabad; *j*=Boordu; *k*=Akkulen; *l,m*=Aktyuz; *n,o*=Makmal; *p, q,r*=Kumtor; *s*=Kokkiya; *t*=Mudryum; *u,v*=Uchkoshkon; *w,x*=Djangart; *y*=Sarysay; *z*=Akshiyrak; *aa*=Shangkelan. Abbreviations: *AS* Altayshan (including Halong unit), *AA* Abagong Arc, *PK* Paleo-Kazakhstan, *NTS* Northern Tien Shan, *NETS* North-Eastern Tien Shan, *MTS* Middle Tien Shan, *STS* Southern Tien Shan, *IR* Irtysh fault, *AR* Armantai Suture, *NL* Nikolaev Line, *STSS* Southern Tien Shan Suture, *TF* Talas-Farghona strike-slip fault. The *dashed line* represents the state border between China, Mongolia, and Former Soviet Union (FSU) republics

structural units or terranes (Zonenshain et al. 1990; Fig. 2): (1) the Northern Tien Shan (NTS), which is the deformed margin of the Caledonian Paleo-Kazakhstan continent; (2) the Middle Tien Shan (MTS), which is a Late Paleozoic volcano-plutonic arc; and (3) the Southern Tien Shan (STS), which is an intensely deformed fold-and-thrust belt formed after the final closure of the Paleo-Turkestan ocean.

The subdivision into Northern, Middle, and Southern Tien Shan used for the Uzbek and Kyrgyz parts of the Tien Shan does not coincide exactly with that used for the Chinese part of the Tien Shan (e.g., Chen et al. 1999). The Middle Tien Shan, represented in Uzbekistan and Kyrgyzstan by the Beltau-Kurama arc, thins out and does not continue further east in the Chinese part of the Tien Shan (Fig. 2). In contrast, the Middle or Central Tien Shan, including the Yili micro-continent, in the Chinese literature corresponds to the Northern Tien Shan of Kyrgyzstan, while the Northern Tien Shan in China is bound to the Caledonian Paleo-Kazakhstan itself. In this paper, we follow the subdivision used in the Russian literature for Kyrgyzstan because our sampling was concentrated in this country and because east of the Talas-Farghona strike-slip fault (Fig. 2) there is no principal difference in basement structures of the Middle and Northern Tien Shan, and the southern terranes of Paleo-Kazakhstan.

The Northern Tien Shan is a part of the Caledonian Paleo-Kazakhstan plate represented in the Kyrgyz territory by the Early Paleozoic arc and its Precambrian basement intruded by voluminous Ordovician granitoids. The main component of the Middle Tien Shan is the Carboniferous Beltau-Kurama volcano-plutonic belt developed on Pre-

cambrian basement. This belt is usually considered either as an active continental margin of the Paleo-Kazakhstan or as a mature volcanic arc that was accreted to the Paleo-Kazakhstan margin approximately 320 Ma ago (e.g., Yakubchuk et al. 2002). In Kyrgyzstan, the Northern and Middle Tien Shan are separated by the Nikolaev Line, a Hercynian strike-slip fault generally following a Caledonian suture (Fig. 2). The Southern Tien Shan includes intensely deformed fore-arc accretionary complexes together with passive margin sediments of the Karakum-Tarim continent.

The Middle and Southern Tien Shan terranes are separated by the Hercynian Southern Tien Shan Suture (Fig. 2), defined by ophiolites with ages ranging from Lower Ordovician to Early Carboniferous (Biske et al. 1998; Jun et al. 1998; Chen et al. 1999). In Uzbekistan, Tadjikistan, and Kyrgyzstan, the southern Tien Shan is tentatively divided into three segments from west to east: Kyzylkum, Alay, and Kokshaal (Fig. 2). The Talas-Farghona dextral strike-slip fault separates the western terranes of the Tien Shan, namely, the Kyzylkum and Alay segments of the Southern Tien Shan (STS-W) and the Kurama range of the Middle Tien Shan (MTS-W), from the eastern terranes (Kokshaal Segment of the Southern Tien Shan or STS-E, Middle Tien Shan east of the Talas-Farghona fault or MTS-E, and Northern Tien Shan east of the Talas-Farghona fault or NTS-E) (Fig. 2).

An eye-catching feature of the present day Tien Shan geology is a number of major east–west striking trans-crustal shear zones dividing the Tien Shan into a series of tectonic blocks (Fig. 2). These shear zones are oblique or

parallel to the Hercynian Southern Tien Shan Suture and control the post-collisional magmatism and important mineralization (e.g., Mao et al. 2004).

The Chinese Altay

The Altay orogenic belt is situated at the junction of the state boundaries between China, Kazakhstan, and Russia in the west, and China, Mongolia, and Russia in the east (Fig. 2). Windley et al. (2002) and Xiao et al. (2004) subdivided the Chinese and Mongolian parts of the Altay into 11 tectonostratigraphic units. Most units were developed in subduction-related environments and were accreted from the Cambrian to the Permian to the north (present coordinates), making the whole orogen progressively younger to the south. The oldest unit, which may be correlated with the Gorny (Mountain) Altay terrane of the Russian part of Altay, is represented by the Early Proterozoic core, that was rifted off the Siberian Craton during the Late Proterozoic and became the basement of a continental island arc during the Cambrian and Early Ordovician. During the Caledonian collision, this continental island arc was accreted back to the Siberian margin together with the other fragments of the Siberian Craton comprising the core of the East Sayan orogenic belt (Fig. 1) and several smaller Precambrian blocks. After the Caledonian collision, the Altay and the East Sayan belts represented a single young plate against which Devonian-Early Carboniferous arcs, formed in the Junggar-Balkhash ocean, were accreted during the Mid- and Late Paleozoic collisions.

In the Chinese Altay, this Caledonian plate is represented by the Altayshan unit (Xiao et al. 2004), south of which the Halong unit, another Precambrian micro-continent, was accreted in the Late Devonian (Xiao et al. 2004). A Late Silurian–Early Devonian island arc, the Abagong unit, was accreted in the Late Devonian south of the Halong unit. The Abagong island arc hosts most of the volcanic-hosted massive sulfide (VHMS) and orogenic gold deposits (e.g., Goldfarb et al. 2003) sampled in this study and correlates with the Rudny (Ore) Altay terrane situated in the Kazakh and Russian parts of the Altay orogen. South of the Abagong arc the transcrustal strike-slip Irtysh (Erqis) fault developed along the Hercynian suture between the Altay, Paleo-Kazakhstan, and the remnants of the Junggar-Balkhash oceanic plate, probably underlying Mesozoic sediments of the Junggar basin (Fig. 2). According to Xiao et al. (2004), three more units comprising Devonian to Carboniferous island arcs with ocean floor remnants are situated south of the Irtysh fault. Similar to the Tien Shan, the terranes of the Altay are separated by major strike-slip faults.

Timing of Hercynian collisional events

Estimates of the age of the Tarim–Paleo-Kazkhstan collision vary from Late Devonian to Late Carboniferous–Early Permian (Windley et al. 1990; Allen et al. 1992; Biske et al. 1998; Chen et al. 1999; Carroll et al. 2001; Zhou et al. 2001). Thick Early Permian molasses mark the final closure of the Paleo-Turkestan ocean and uplift. Several authors highlight the "soft" or oblique and apparently scissors-like (from east to west) character of the collision between Tarim and Paleo-Kazkhstan (e.g., Chen et al. 1999). The closure of a separate Junggar-Balkhash branch of the Paleo-Turkestan ocean also occurred by the Early Permian and resulted in docking of the Junggar terranes to Altay and Paleo-Kazakhstan (Feng et al. 1989) and final amalgamation of the southern Altaids. The collision was followed by the formation of the major strike-slip faults already in the Early Permian (Laurent-Charvet et al. 2003). These faults controlled the emplacement of the granitoid intrusions and ore deposits in the post-collisional stage.

After the collision, a tectonically quiet period followed until the Mesozoic extension, accompanied by granitoid magmatism and elevated heat flow. In the investigated area, Mesozoic metamorphism and granitoid intrusions are known in the Kyzylkum Segment of the Southern Tien Shan (STS-W) and in the Chinese Altay (Kostitsyn 1996; Hong et al. 2003).

Metallogenic evolution of the Tien Shan and Altay

The major ore deposits of the Tien Shan and Altay were formed in the Middle and Late Paleozoic, whereas the Early Paleozoic deposits are few (Table 1 and Fig. 2). Many of the ore deposits, especially those formed in the post-collisional stage, are associated with granitoid intrusions (Table 2 and Fig. 2).

During the Devonian and Carboniferous, the time span that preceded the Hercynian collision, volcanic-hosted massive sulfide (VHMS) deposits (Ashele, Keketale, and Mengku) were formed in intra-oceanic island arcs and remnants of the oceanic crust in the Chinese Altay (Rui et al. 2002). In contrast, in the North and Middle Tien Shan terranes the majority of the Devonian and Carboniferous ore deposits were formed in an active continental margin environment (Jenchuraeva 1997, 2001; Table 1). The predominant deposit types include intrusion-related Cu–Bi–Au, REE, Au deposits associated with Devonian (Axi deposit in the Chinese NTS-E, Aktyuz and Boordu in the Kyrgyz NTS-E: Shatov, personal communication, 2005) and Early Permian (Taldybulak Levoberezhny in the Kyrgyz NTS-E) granites of the southern and eastern Paleo-Kazakhstan margins, and epithermal volcanic-hosted Au–Ag–Te, porphyry Cu–Mo–Au, and base metal deposits associated with Carboniferous and Early Permian subduction-related calc-alkaline magmatic rocks of the continental Beltau-Kurama arc (Kalmakyr, Kochbulak, and Ustarasay deposits in the Uzbek part of the Beltau-Kurama arc, MTS-W). This stage is also represented by the Uchkulach stratabound base metal deposit situated in the eastern part of the Middle Tien Shan in the south Kyzylkum desert of Uzbekistan (MTS-W; Table 1).

Table 1 Deposits analyzed in the present study subdivided by terrane

Deposit	Type	Metals	Age (Ma)	Country	Coordinates	Environment	Ref.
Kyzylkum segment of Southern Tien Shan (STS-W)							
Sarytau	Intrusion-related	Au, W	278	Uzbekistan	42°11′48″N, 64°11′46″E	Post-collisional	1
Muruntau	S Orogenic Au	Au	286–260	Uzbekistan	41°30′51″N, 64°34′33″E	Post-collisional	2a, 3
Amantaitau	S Orogenic Au	Au	270–260	Uzbekistan	41°19′52′N, 6418′58″E	Post-collisional	2b
Daugyztau	S Orogenic Au	Au	270–260	Uzbekistan	41°16′53″N, 64°15′05″E	Post-collisional	2c
Guzhumsay	S Orogenic Au	Au	280?	Uzbekistan	40°25′41″N, 65°50′13″E	Post-collisional	4
Sarmich	Orogenic Au	Au	280?	Uzbekistan	40°21′38″N, 65°46′30″E	Post-collisional	4, 5
Zarmitan	I Orogenic Au	Au	269	Uzbekistan	40°19′34″N, 66°44′18″E	Post-collisional	2d, 6
Mardjanbulak	S Orogenic Au	Au	280?	Uzbekistan	39°57′02″N, 67°22′16″E	Post-collisional	4
Middle Tien Shan west of Talas-Farghona fault (MTS-W)							
Uchkulach	Stratabound	Zn, Pb	UP	Uzbekistan	40°29′52″N, 67°21′06″E	Shelf/back arc?	4
Kalmakyr	Porphyry-Cu	Cu, Au	310	Uzbekistan	40°47′39″N, 69°40′26″E	Continental arc	2e
Kochbulak	epithermal	Au, Ag, Te	290–280	Uzbekistan	40°37′16″N, 70°08′31″E	Continental arc	2f
Ustarasay	Intrusion-related	W, Bi, (±Au)	UP	Uzbekistan	41°32′53″N, 70°46′31″E	Continental arc	7
Northern Tien Shan east of Talas-Farghona fault (NTS-E)							
Boordu	Intrusion-related	Pb, Zn (±Au)	UP	Kyrgyzstan	42°39′26″N, 75°34′51″E	Continental arc	12
Taldybulak Levoberezhny	Epithermal	Au, Ag	UP	Kyrgyzstan	42°38′28″N, 75°40′41″E	Continental arc	13
Aktyuz	Intrusion-related	REE + Au	416	Kyrgyzstan	42°52′37″N, 76°10′40″E	Continental arc	11
Axi	Epithermal	Au	350	Xinjiang, China	44°13′48″N, 81°36′25″E	Continental arc	14
Middle Tien Shan east of Talas-Farghona fault (MTS-E)							
Makmal	Skarn	Au	280	Kyrgyzstan	41°10′52″N, 73°59′22″E	Post-collisional	2h, 10
Kumtor	S Orogenic Au	Au	280	Kyrgyzstan	41°50′57″N, 78°10′51″E	Post-collisional	2g, 8, 9
Altay							
Manka	Intrusion-related	Au, W	UP	Kazakhstan	48°31′23″N, 85°48′19″E	Post-collisional	7
Ashele	VHMS	Cu, Zn	~380	Xinjiang, China	48°16′34″N, 86°19′44″E	Island arc	15
Saidu	S Orogenic Au	Au	280	Xinjiang, China	48°09′07″N, 86°32′9″E	Post-collisional	19
Shangkelan	Pegmatite	Rare metals	180	Xinjiang, China	47°56′54″N, 88°09′56″E	Intra-plate	20
Mengku	VHMS-skarn	Fe	~380	Xinjiang, China	47°31′54″N, 88°58′46″E	Island arc	18
Keketale	VHMS	Pb, Zn	280	Xinjiang, China	47°20′58″N, 89°11′58″E	Continental rift	17
Kalatonge	Magmatic Cu–Ni	Cu, Ni	280	Xinjiang, China	46°45′39″N, 89°40′32″E	Post-collisional	16

UP Upper Paleozoic, *VHMS* volcanic-hosted massive sulfide, *S* sediment-hosted, *I* intrusion-hosted

1=Konopelko et al. (2003b); 2a, b, c, d, e, f, g=Yakubchuk et al. (2002) and references therein. 2a: 175 Moz Au; 2b: 4 Moz Au; 2c: 4 Moz Au; 2d: 11.3 Moz Au; 2e: 93 Moz Au; 2f: 4.3 Moz Au; 2g: 19 Moz Au; 2h: 2 Moz Au; 3=Morelli et al. (2004); 4=Seltmann et al. (2005); 5=Askerova (1996); 6=Bortnikov et al. (1996); 7=Chiaradia (2003); 8=Jenchuraeva et al. (2001a); 9=Ansdell et al. (1999); 10=Jenchuraeva et al. (2001b); 11=Konopelko and Seltmann (unpublished data); 12=Usmanov (2001); 13=Malyukova (2001); 14=Hart et al. (2003): 1.6–2.3 Moz Au; 15=Wang (2003): 1.08 Mt Cu; 16=Yan et al. (2003): 670 kt Cu and Ni; 17=Wang et al. (2003a); 18=Wang et al. (2003b): 110 Mt at 23.93–57.57 % FeO; 19=Liu et al. (2003); 20=Chen et al. (2000b)

The post-collisional metallogenic evolution of the Tien Shan and Chinese Altay was defined by the thermal event that affected the whole region across terrane boundaries and produced both voluminous post-collisional granitoid intrusions and ore deposits predominantly of the orogenic gold type (e.g., Savchuk et al. 1991; Konopelko et al. 2003a; Mao et al. 2004). Emplacement of post-collisional granites and orogenic gold deposits was controlled by the regional scale strike-slip faults formed after final amalgamation of the southern Altaid orogenic collage in the Early Permian (Laurent-Charvet et al. 2003). The post-collisional deposits of the Altay are characterized by the orogenic and intrusion-related gold deposits of Saidu and Manka in the Chinese and Kazakh Altay, respectively, and by the Kalatonge Cu–Ni deposit in the Chinese Altay

hosted by a Permian gabbroic intrusion (Table 1). The post-collisional deposits of the Tien Shan are represented by a number of orogenic and intrusion-related gold deposits including the Muruntau, Amantaitau, Daugyztau, Sarytau, Zarmitan (hosted by the Koshrabad granite), Guzhumsay, Mardjanbulak, and Sarmich deposits in the Kyzylkum Segment of the Southern Tien Shan (STS-W) and the Kumtor and Makmal gold deposits in the Middle Tien Shan east of the Talas-Farghona fault (MTS-E). To characterize the crust of the Kokshaal Segment of the Southern Tien Shan (STS-E), we sampled six post-collisional intrusions in this area (Table 2) described by Konopelko et al. (2003a). The Mesozoic extension and related magmatism is represented in this work by the pyrite-rich Shangkelan granite sampled in the Chinese Altay.

Table 2 Lithologies analyzed in the present study subdivided by terrane

Sample	Lithology	Material analyzed	Intrusion	Age (Ma)	Country	Coordinates	Environment	Ref.
Kyzylkum segment of Southern Tien Shan (STS-W)								
401200	Aplite granite	L, R	Sarytau	278	Uzbekistan	42°11′48″N, 64°11′46″E	Post-collisional	1
401201	Granite	L, R	Sarytau	278	Uzbekistan	42°11′48″N, 64°11′46″E	Post-collisional	1
12	Schist	L, R	Muruntau	Cambrian	Uzbekistan	41°33′00″N, 64°18′00″E	Back-arc?	2
14a	Schist	L, R	Muruntau	Cambrian	Uzbekistan	41°33′00″N, 64°18′00″E	Back-arc?	2
43	Granite	Kf	Muruntau–Tamdy	290	Uzbekistan	41°40′12″N, 64°18′10″E	Post-collisional	3
44	Granite	Kf	Muruntau–Tamdy	290	Uzbekistan	41°40′12″N, 64°18′10″E	Post-collisional	3
45	Granite	Kf	Muruntau–Tamdy	290	Uzbekistan	41°40′12″N, 64°18′10″E	Post-collisional	3
401700	Granite	Kf	Koshrabad	285	Uzbekistan	40°19′34″N, 66°44′18″E	Post-collisional	4
401701	Granite	Kf	Koshrabad	285	Uzbekistan	40°19′34″N, 66°44′18″E	Post-collisional	4
Northern Tien Shan east of Talas-Farghona fault (NTS-E)								
320300	Granite	Kf, L, R	Boordu	UP	Kyrgyzstan	42°39′26″N, 75°34′51″E	Continental arc	5
Akkulen	Syenite	Kf	Akkulen	290	Kyrgyzstan	42°17′50″N, 76°08′46″E	Post-collisional	6
320000	Granite	WR, L, R	Aktyuz	411	Kyrgyzstan	42°51′35″N, 76°56′05″E	Continental arc	7
320001	Granite	L, R	Aktyuz	411	Kyrgyzstan	42°51′35″N, 76°56′05″E	Continental arc	7
Middle Tien Shan east of Talas-Farghona fault (MTS-E)								
320100	Granite	WR, L, R	Makmal	280	Kyrgyzstan	41°12′00″N, 73°59′57″E	Post-collisional	8
320101	Granite	WR, L, R	Makmal	280	Kyrgyzstan	41°12′00″N, 73°59′57″E	Post-collisional	8
350004	Schist	L, R, py	Kumtor	Vendian	Kyrgyzstan	41°50′57″N, 78°10′51″E	Back-arc?	9
Schist 1	Schist	py	Kumtor	Vendian	Kyrgyzstan	41°50′57″N, 78°10′51″E	Back-arc?	9
Schist 2	Schist	py	Kumtor	Vendian	Kyrgyzstan	41°50′57″N, 78°10′51″E	Back-arc?	9
Kokshaal segement of Southern Tien Shan (STS-E)								
221802	Granite	Kf	Kokkiya	280	Kyrgyzstan	40°47′43″N, 76°19′22″E	Post-collisional	10
220203	Granite	Kf	Mudryum	280	Kyrgyzstan	40°56′10″N, 76°37′21″E	Post-collisional	10
206201	Granite	Kf	Uchkoshkon	279	Kyrgyzstan	41°47′20″N, 78°42′26″E	Post-collisional	10
206802	Granite	Kf	Uchkoshkon	279	Kyrgyzstan	41°48′04″N, 78°42′10″E	Post-collisional	10
208901	Granite	Kf	Djangart	294	Kyrgyzstan	41°39′05″N, 78°50′22″E	Post-collisional	10
209103	Granite	Kf	Djangart	294	Kyrgyzstan	41°39′00″N, 78°50′55″E	Post-collisional	10
209001	Alkaline rock	py	Sarysay	280?	Kyrgyzstan	41°39′50″N, 78°49′23″E	Post-collisional	10
215604	Granite	Kf	Akshiyrak	294	Kyrgyzstan	41°46′32″N, 78°55′47″E	Post-collisional	10
Altay								
xj9	Granite	Kf	Shangkelan	180	Xinjiang, China	47°56′54″N, 88°09′56″E	Intraplate	11

WR Whole rock, *L* leachate, *R* residue, *Kf* K-feldspar (for details on the analytical procedures, see text)
1=Konopelko et al. (2003b); 2=Drew et al. (1996); 3=Kempe et al. (2004); 4=Bortnikov et al. (1996); 5=Usmanov (2001); 6=Jenchuraeva (2001); 7=Shatov (personal communication); 8=Jenchuraeva et al. (2001b); 9=Abeleira et al. (2000); 10=Konopelko et al. (2003a); 11=Chen et al. (2000b)

Interpretation models for Pb isotopes

Lead isotopes are a powerful tool to trace the sources of metals in ore deposits and to discriminate terranes (e.g., Zartman 1974; Wörner et al. 1992; Macfarlane et al. 1990; Chiaradia et al. 2004). The advantages of the Pb isotope system over the Sr and Nd systems are twofold: (1) Pb isotope compositions can be easily measured not only on rocks but also on ore minerals, thus providing an insight on the interaction of hydrothermal fluids (and not only magmas) with the crustal basement and on the metal sources for ore deposits; and (2) three radiogenic Pb isotopes (^{206}Pb, ^{207}Pb, ^{208}Pb) are derived from three different radioactive nuclides (^{238}U, ^{235}U, ^{232}Th respectively), thus allowing investigation of the Pb isotope system in a tridimensional space compared to the unidimensional space of the Sr rand Nd systems character-

ized by only one radiogenic isotope (^{87}Sr and ^{143}Nd derived from ^{87}Rb and ^{147}Sm, respectively).

In metallogenic studies, it is necessary to know the lead isotope composition of the ore minerals at the time of their formation (common lead isotope composition) for a correct interpretation of the data. This can be obtained by analysing Pb-rich minerals (most commonly galena) that virtually "freeze" the isotopic composition of the reservoir from which they derive at the moment of their formation due to the low U/Pb and Th/Pb ratios. Among silicate minerals, also K-feldspars retain mostly the common lead signature due to their low U/Pb and Th/Pb ratios (Carignan et al. 1993). However, in all other minerals (Pb-poor systems), especially those older than the Mesozoic, a correction for time-integrated decay of U and Th, incorporated into the mineral at the time of its formation and producing in situ radiogenic lead, might be required to obtain the common lead signature

(e.g., Tosdal et al. 1999). The entity of this correction will depend on the $^{238}U/^{204}Pb$ ($=\mu$) and $^{232}Th/^{204}Pb$ ($=\omega$) values and the age of the mineral.

The common lead isotope signatures of ore minerals can be interpreted in terms of derivation from one or more large-scale terrestrial reservoirs (e.g., upper and lower crust, mantle) or, in a more detailed way, in terms of derivation from regional reservoirs, i.e., country rocks. The first option requires the use of model evolution curves that simulate the tridimensional Pb isotopic evolution through

time of different terrestrial reservoirs based on the geochemical partitioning of U, Th, and Pb during geological processes. One of the most used models is that of Zartman and Doe (1981) that highlights the evolutions through time of the upper crust, lower crust, and mantle reservoirs in the uranogenic ($^{207}Pb/^{204}Pb$ vs $^{206}Pb/^{204}Pb$) and thorogenic ($^{208}Pb/^{204}Pb$ vs $^{206}Pb/^{204}Pb$) plots (Figs. 3 and 4). In the uranogenic plot, the upper crust evolution curve has the highest $^{207}Pb/^{204}Pb$ values due to the U enrichment (high $\mu=^{238}U/^{204}Pb$ values) of upper crustal

Fig. 3 $^{207}Pb/^{204}Pb$ vs $^{206}Pb/^{204}Pb$ and $^{208}Pb/^{204}Pb$ vs $^{206}Pb/^{204}Pb$ diagrams of whole rocks fractions (leachate and residues) and minerals (K-feldspars, sulfides) investigated in this study. The upper crust (*UC*), orogen (*OR*), and mantle (*M*) evolution curves are from Zartman and Doe (1981). *Arrows* connect residue–leachate pairs of whole rocks
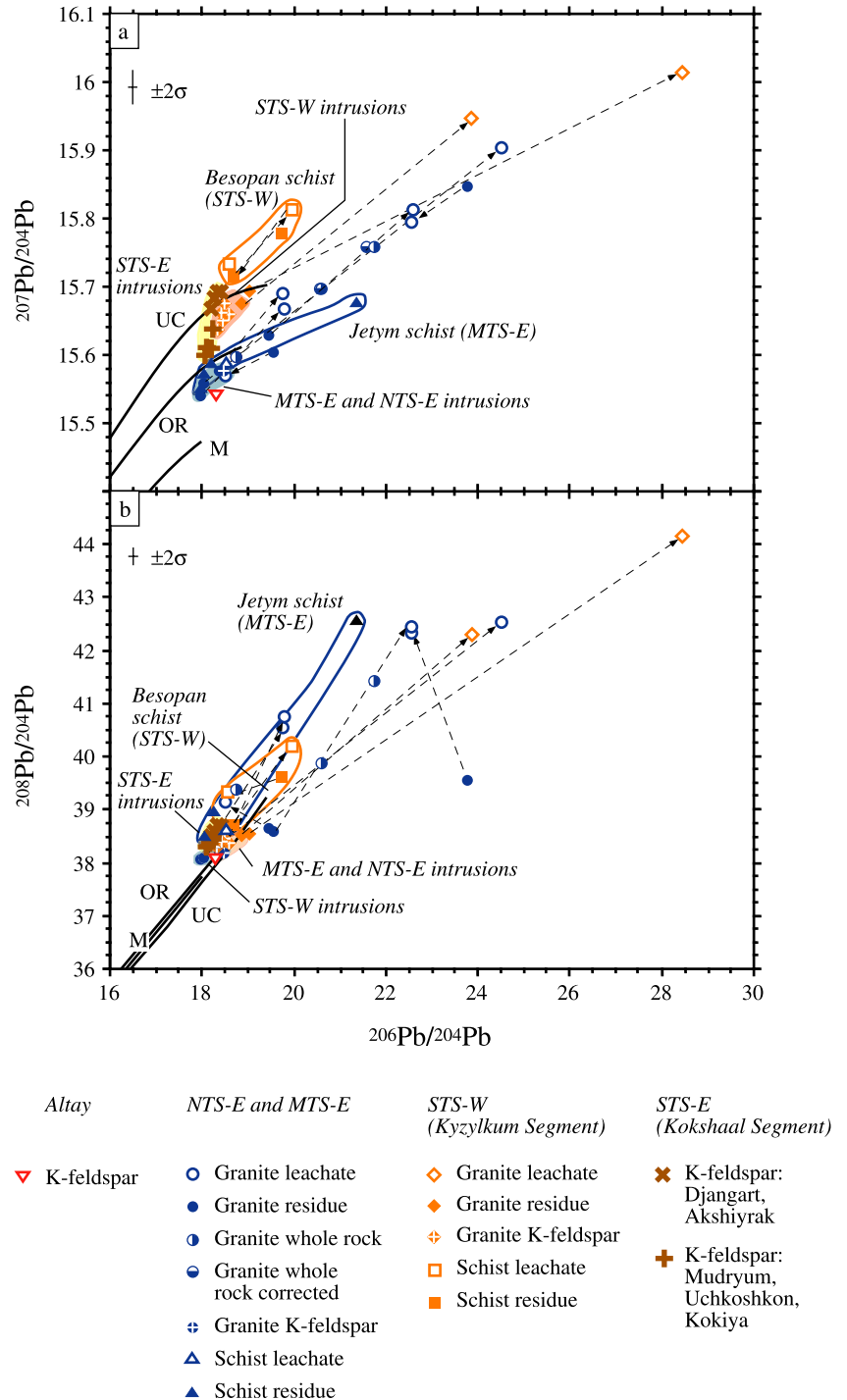
lithologies during mantle-to-crust magma transfer processes. Conversely, the residual mantle evolution curve has low $^{207}Pb/^{204}Pb$ values due to progressive loss of U to the upper crust. The lower crust evolution curve has even lower $^{207}Pb/^{204}Pb$ values due to the high mobility of U during high-grade metamorphism affecting lower crust rocks, resulting in very low μ ($^{238}U/^{204}Pb$) values. The thorogenic plot is useful to discriminate the evolution of the lower crust reservoir from that of the upper crust and mantle reservoirs, because the former is characterized by high $^{208}Pb/^{204}Pb$ values for similar $^{206}Pb/^{204}Pb$ values due to the relative immobility of Th (compared to U) during

high-grade metamorphism affecting lower crust rocks, which results in comparatively high ω ($=^{232}Th/^{204}Pb$) values. The $^{208}Pb/^{204}Pb$ values of lower crust-type rocks are increasingly higher, for the same $^{206}Pb/^{204}Pb$ value, as the age of the high-grade metamorphism is increasingly older, because this allows rocks to evolve for a longer time with a high ω value.

The second option (evaluation of regional reservoirs) requires the analysis of the isotopic compositions of country rocks to compare them with the isotopic compositions of the ores. Magmatic rocks that are coeval with a mineralization can deliver to ore fluids only their common

Fig. 4 $^{207}Pb/^{204}Pb$ vs $^{206}Pb/^{204}Pb$ and $^{208}Pb/^{204}Pb$ vs $^{206}Pb/^{204}Pb$ diagrams of ore minerals investigated in this study subdivided by terrane. The *colored areas* represent the compositional fields of whole rocks from Fig. 3. The upper crust (*UC*), orogen (*OR*), and mantle (*M*) evolution curves are from Zartman and Doe (1981). *Arrows* connect raw and time-integrated corrected values (*tip of the arrows*) of the same ore minerals. Age-corrected values are based on the ore deposit ages reported in Table 1
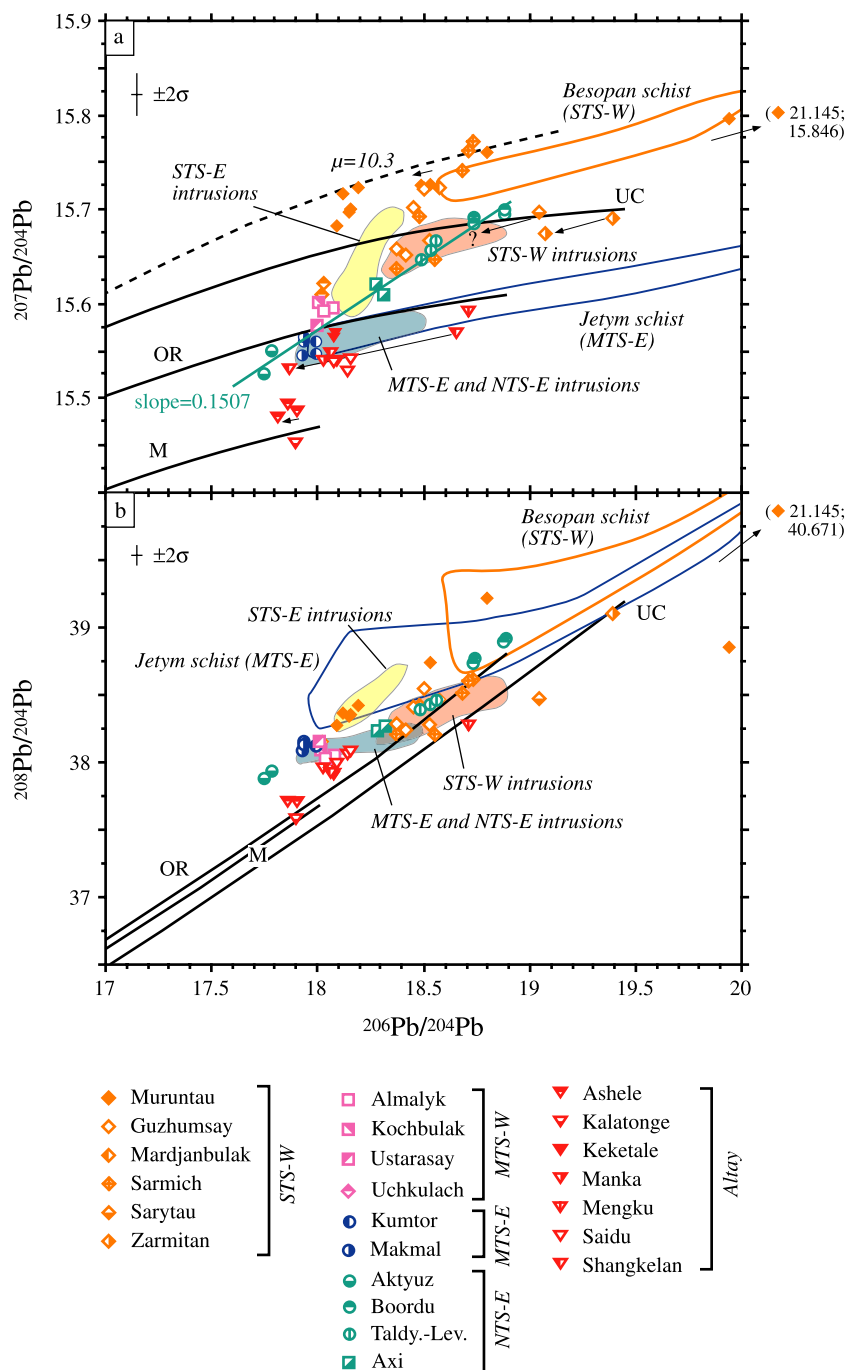
lead, whereas basement rocks (metamorphic, magmatic, and sedimentary) older than the mineralization will deliver to ore fluids a mixture of common and radiogenic lead. Common lead of magmatic rocks can be obtained from K-feldspars, time-integrated correction for U (and Th) decay of raw isotopic ratios and, to some extent, from analyses of residual rock fractions (Chiaradia and Fontboté 2003). In contrast, separate leachate and residue analyses may give more information than single whole-rock analyses about the lead contributed by basement lithologies to ore fluids (e.g., Gulson 1977; Curti 1987; Macfarlane and Petersen 1990; Chiaradia and Fontboté 2003).

Analytical techniques

We have measured lead isotope compositions of 59 sulfide samples from 25 mineral deposits (Tables 1 and 3; Fig. 2) as well as of 47 rock, K-feldspar, and magmatic-hydrothermal sulfide samples from 25 whole rocks including granitoids (N=21) and low-grade metasedimentary schists (N=3) (Tables 2 and 4; Fig. 2). To obtain the common lead signature of the ores, galena was analyzed whenever possible (N=22), otherwise, pyrite, chalcopyrite, tetrahedrite, and scheelite were analyzed (N=37). In the latter case, U and Pb concentrations were measured by isotope dilution on TIMS (see below) for most samples (N=22) and a correction for U decay was made, because the investigated sulfides are from Paleozoic ore deposits (except Shangkelan, which is Mesozoic). We have tried to obtain the common lead signatures of intrusions from K-feldspars, magmatic-hydrothermal pyrite, time-integrated corrections for U decay of raw isotopic ratios, and from analyses of residual rock fractions (Chiaradia and Fontboté 2003) (Table 4). We have also carried out leachate analyses on metasedimentary basement rocks to evaluate their potential lead contribution to ore fluids.

A few tens of milligrams of sulfide minerals and a mixed ^{202}Pb/^{236}U spike were dissolved and homogenized overnight in sealed Teflon beakers at 180°C with 2 ml of 7 M HCl and 1 ml of 15 M HNO$_3$, whereas a tiny amount of galena was directly dissolved in 15 M HNO$_3$.

When corrected to their intrusion ages (Table 2) for time-integrated decay of U, magmatic rock powders were added a mixed ^{202}Pb/^{236}U spike and digested in a mixture of concentrated HNO$_3$ and HF during a few days. Otherwise, rock powders and K-feldspars were subjected to a strong acid leaching (i.e., ≥36 h at 180°C in screw-sealed 20-ml Teflon beakers using a mixture of 3.5 ml of 7 M HCl and 1.5 ml of 14 M HNO$_3$; Chiaradia and Fontboté 2003). The residual fractions were rinsed twice with deionized water and digested for ≥48 h at 180°C in sealed Teflon beakers using a mixture of concentrated HNO$_3$ and HF. Lead and (when applicable) uranium of sulfides (except galena), leachate and residue rock fractions as well as whole rocks and residues of K-feldspars were purified by chromatography with AG-MP1 resin in hydrobromic medium and with AG1-X8 resin in nitric acid medium, respectively. Leachates of K-feldspars were discarded.

Lead fractions of the purified sulfide, rock, and K-feldspar as well as of the dissolved galena were loaded onto rhenium filaments using the silica gel technique. Lead isotope compositions were measured statically on a multicollector Finnigan TRITON mass spectrometer at a pyrometer-controlled filament temperature of 1,210°C at the Centre for Geochemical Mass Spectrometry (University of Leeds, UK). Lead isotope compositions were corrected for fractionation by a +0.08% amu correction factor based on 60 analyses of the SRM981 international standard using the SRM981 values of Todt et al. (1996). The external reproducibilities (2σ) of the SRM981 standard are 0.08% for ^{206}Pb/^{204}Pb, 0.13% for ^{207}Pb/^{204}Pb and 0.17% for ^{208}Pb/^{204}Pb. Procedural blanks ranged between 64 and 120 pg Pb. Uranium concentrations were measured by isotope dilution by determining uranium isotope ratios in multidynamic mode on the secondary electron multiplier and on Faraday cups.

Results

Plutonic rocks

Time-integrated decay corrections of whole rocks and analyses of leachate-residue pairs have been carried out for samples 320000 (Aktyuz granite), 320100 (Makmal granite), and 320101 (Makmal granite). Time-integrated decay corrections of these samples fail to yield the common lead because of probable U loss, a typical problem of medium- to coarse-grained granites in surficial weathering environments (Tosdal et al. 1999). In contrast, residual fractions of the Makmal fresh granite samples (320100 and 320101) are identical to Pb isotope compositions of common lead of pyrite from the associated mineralization (see Tables 3 and 4). The residue fraction of the altered Aktyuz granite sample (320000) is less radiogenic than the corrected values of the whole rock but is significantly more radiogenic than the leachate fraction. This feature is typical of hydrothermally altered magmatic rocks (Marschik et al. 2003) and the residue fraction obviously does not represent the common lead. The residual fraction of sample 320300 (Boordu granite) is slightly less radiogenic than a K-feldspar from the same rock and, thus, should also represent the common lead. Residual fractions of Sarytau granite samples (401200 and 401201) are less radiogenic than corresponding leachates and might approximate the common lead signature, but, in the absence of common lead compositions of associated K-feldspar/sulfide, we cannot exclude that they contain some radiogenic lead.

The common Pb isotope signatures (i.e., rock residues, excluding the samples discussed above, and K-feldspars) of the intrusive rocks of different Tien Shan segments plot in separate fields within conventional isotope diagrams (Fig. 3). MTS-E and NTS-E intrusions plot in a narrow field slightly below the orogen curve of Zartman and Doe (1981) in the uranogenic plot and slightly above it in the thorogenic plot (Fig. 3). In contrast, the intrusions of the STS-W straddle the upper crust curve of Zartman and Doe

Table 3 Lead isotope compositions and U and Pb concentrations of sulfides from the ore deposits of Table 1

Sample	Mineral	$^{206}Pb/^{204}Pb$	$^{207}Pb/^{204}Pb$	$^{208}Pb/^{204}Pb$	Pb (ppm)[1]	U (ppm)[1]	$^{206}Pb/^{204}Pb_{cor}$[2]	$^{207}Pb/^{204}Pb_{cor}$[2]	Deposit
Kyzylkum segment of Southern Tien Shan (STS-W)									
401500	py	18.118	15.716	38.369	150	0.08	*18.118*	*15.716*	Amantaitau
401501	py	18.534	15.726	38.740	55	0.87	*18.491*	*15.724*	Amantaitau
MUZ4	cpy	18.193	15.723	38.424	n.d.	n.d.	–	–	Amantaitau
MUZ5	cpy	18.156	15.700	38.348	n.d.	n.d.	–	–	Amantaitau
MUZ1	py	18.800	15.761	39.221	n.d.	n.d.	–	–	Daugyztau
MUZ3a	py	18.090	15.682	38.269	n.d.	n.d.	–	–	Daugyztau
MUZ3b	py	18.149	15.698	38.343	n.d.	n.d.	–	–	Daugyztau
MUZ3c	py	18.102	15.672	38.304	n.d.	n.d.	–	–	Daugyztau
MUZ6	cpy	19.942	15.796	38.848	n.d.	n.d.	–	–	Muruntau
MUZ7	cpy	21.145	15.846	40.671	n.d.	n.d.	–	–	Muruntau
gn27	gn	18.528	15.668	38.273	–	–	–	–	Guzhumsay
gn28	gn	18.454	15.702	38.407	–	–	–	–	Guzhumsay
gn29	gn	18.373	15.658	38.285	–	–	–	–	Guzhumsay
gn30	gn	18.418	15.651	38.242	–	–	–	–	Guzhumsay
gn31	gn	18.503	15.722	38.549	–	–	–	–	Guzhumsay
gn2	gn	18.574	15.723	38.468	–	–	–	–	Mardjanbulak
gn14	gn	18.485	15.692	38.422	–	–	–	–	Sarmich
gn16	gn	18.716	15.762	38.601	–	–	–	–	Sarmich
gn17	gn	18.553	15.646	38.199	–	–	–	–	Sarmich
gn18	gn	18.370	15.637	38.208	–	–	–	–	Sarmich
gn20	gn	18.737	15.772	38.612	–	–	–	–	Sarmich
gn21	gn	18.684	15.741	38.513	–	–	–	–	Sarmich
401205	py	19.049	15.697	38.464	3.2	33.48	*(−10.196)*	*(14.181)*	Sarytau
410701	py	19.395	15.690	39.101	58	6.78	*(19.077)*	*(15.674)*	Zarmitan
Middle Tien Shan west of Talas-Farghona fault (MTS-W)									
MUZ10	cpy	18.079	15.594	38.056	n.d.	n.d.	–	–	Kalmakyr
MUZ9	cpy	18.035	15.592	38.037	n.d.	n.d.	–	–	Kalmakyr
MUZ12	tetr	18.010	15.601	38.105	n.d.	n.d.	–	–	Kochbulak
400001a	gn	18.022	15.623	38.155	–	–	–	–	Uchkulach
400001b	gn	18.042	15.651	38.257	–	–	–	–	Uchkulach
UST1[c]	sch	18.004	15.577	38.161	n.d.	n.d.	–	–	Ustarasay
Northern Tien Shan east of Talas-Farghona fault (NTS-E)									
320002	py	17.783	15.551	37.937	1843	0.28	*17.782*	*15.551*	Aktyuz
320003	py	17.743	15.527	37.885	13661	5.60	*17.742*	*15.527*	Aktyuz
320301	gn	18.876	15.696	38.901	–	–	–	–	Boordu
320301-rep	gn	18.876	15.701	38.910	–	–	–	–	Boordu
320303	gn	18.732	15.685	38.744	–	–	–	–	Boordu
320303-rep	gn	18.737	15.692	38.768	–	–	–	–	Boordu
TBLB5053	gn	18.553	15.667	38.453					Taldybulak
TBLB5053	py	18.535	15.658	38.430	7726	0.06	*18.535*	*15.658*	Taldybulak
TBLB5050	cpy	18.489	15.648	38.409	170	0.02	*18.489*	*15.648*	Taldybulak
xj20	gn	18.283	15.620	38.242	–	–	–	–	Axi
xj21	py	18.319	15.609	38.277	100	0.06	*18.317*	*15.609*	Axi
Middle Tien Shan east of Talas-Farghona fault (MTS-E)									
350002	py	17.993	15.560	38.130	188	0.34	*17.988*	*15.560*	Kumtor
320102	py	17.923	15.546	38.092	61609	0.08	*17.923*	*15.546*	Makmal
320103	py	17.934	15.566	38.156	475	0.03	*17.934*	*15.566*	Makmal
320103-rep	py	17.931	15.561	38.142	473	0.03	*17.931*	*15.561*	Makmal
Altay									
xj18	py	17.907	15.484	37.691	121	2.92	*17.816*	*15.479*	Ashele
xj15	cpy	17.859	15.491	37.693	26946	3.96	*17.858*	*15.491*	Ashele
xj1	py	17.900	15.450	37.565	59	0.02	*17.899*	*15.450*	Kalatonge

Table 3 (continued)

Sample	Mineral	$^{206}Pb/^{204}Pb$	$^{207}Pb/^{204}Pb$	$^{208}Pb/^{204}Pb$	Pb (ppm)[1]	U (ppm)[1]	$^{206}Pb/^{204}Pb_{cor}$[2]	$^{207}Pb/^{204}Pb_{cor}$[2]	Deposit
MNK3[c]	sch	18.025	15.538	37.939	n.d.	n.d.	–	–	Manka
xj2	gn	18.078	15.562	37.890	–	–	–	–	Keketale
xj4a	gn	18.082	15.567	37.906	–	–	–	–	Keketale
xj7	py	18.713	15.590	38.257	6	0.03	*18.695*	*15.589*	Mengku
xj11	py	18.077	15.536	37.982	69	0.32	*18.064*	*15.536*	Saidu
xj12	py	18.091	15.538	37.982	41	0.05	*18.088*	*15.537*	Saidu
xj14	py	18.157	15.539	38.064	180	n.d.			Saidu
xj14-rep	py	18.142	15.527	38.049	174	n.d.			Saidu
xj9a	py	18.064	15.546	37.908	281	0.52	*18.061*	*15.546*	Shangkelan
xj9b	py	23.404	15.824	50.621	0.5	13.5	*(−34.475)*	*(12.948)*	Shangkelan
xj10	py	18.653	15.570	38.092	1.2	0.57	*(17.869)*	*(15.531)*	Shangkelan

Values corrected for U decay at the age of the mineralization (Table 1) are reported in italics. Over- and under-corrected values indicating an open system behavior are within brackets

n.d. not determined, *rep* repeated, *py* pyrite, *cpy* chalcopyrite, *gn* galena, *tetr* terahedrite, *sch* scheelite

[a]Measured by isotope dilution on TIMS

[b]Isotopic ratios corrected for time integrated decay of U using the ages reported in Table 1 and the U and Pb concentrations reported in this Table. The corrected $^{208}Pb/^{204}Pb$ ratio has not been calculated because Th concentrations were not measured

[c]From Chiaradia (2003)

(1981) in both conventional isotope plots and have higher $^{206}Pb/^{204}Pb$ values than those of the MTS-E and NTS-E granites (Fig. 3). Finally, intrusions of the STS-E define a steep trend between the orogen and upper crust evolution curves in the uranogenic diagram and have higher $^{208}Pb/^{204}Pb$ values than intrusions of the STS-W, MTS-E, and NTS-E (Fig. 3). The K-feldspar of the Shangkelan intrusion (Altay) has a low $^{207}Pb/^{204}Pb$ value similar to the least radiogenic compositions of the MTS-E and NTS-E intrusions (e.g., Makmal granite) (Fig. 3). Leachates, which do not have genetic significance (Chiaradia and Fontboté 2003), plot at more radiogenic values than residues and K-feldspars (Fig. 3).

Metasedimentary rocks

Lead isotope analyses have been carried out on the schists of the Vendian Jetym Group in the Kumtor region (MTS-E) and of the Cambrian Besopan Group in the STS-W, which are the hosts of the orogenic gold deposits of Kumtor and Muruntau (Table 1), respectively. In both cases, leachate and residue fractions of the schists define shallow slope trends in the uranogenic plot (Fig. 3). Leachates are either more or less radiogenic than the corresponding residues, an unsystematic behavior that is typical of low-grade metasediments (Chiaradia and Fontboté 2003). The schists of the Vendian Jetym Group (MTS-E), including a sample of syngenetic disseminated pyrite, overlap the field of the MTS-E and NTS-E intrusions and plot on its prolongation along and beyond the orogen curve of Zartman and Doe (1981) in the uranogenic diagram (Fig. 3). In contrast, the Cambrian Besopan schists (STS-W) plot at significantly higher $^{207}Pb/^{204}Pb$ values (Fig. 3).

Ore minerals

The great majority of the sulfide samples analyzed for U and Pb concentrations (N=18 of 22) have very low μ ($^{238}U/^{204}Pb$) values, and time-integrated corrections are insignificant (Table 3). Only samples xj9b and xj10 (Shangkelan), 401205 (Sarytau), and 410701 (Zarmitan) display corrected values that are significantly less (even negative $^{206}Pb/^{204}Pb$ values) or more radiogenic than the common lead values of sulfides of the same deposit (Table 3), suggesting an open-system behavior, and, therefore, have been excluded from the discussion.

Lead isotope compositions of ore deposits of the investigated terranes plot within distinct intervals of $^{207}Pb/^{204}Pb$ values (Fig. 4a). The STS-W Late Paleozoic orogenic Au deposits (Muruntau, Amantaitau, Daugyztau, Guzhumsay, Sarmich, Zarmitan) have the highest $^{207}Pb/^{204}Pb$ compositions straddling the upper crust evolution curve (Fig. 4a). The radiogenic $^{206}Pb/^{204}Pb$ values of two Muruntau and one Daugyztau samples (MUZ1, MUZ6, MUZ7) are likely due to the Pb-poor nature of these ores, which have not been corrected for U decay (Table 3).

Porphyry–Cu and epithermal deposits (Kalmakyr, Kochbulak, Ustarasay) formed in the Beltau-Kurama continental arc of Devonian-Carboniferous age and the stratabound Zn–Pb mineralization of Uchkulach (MTS-W) define a tight cluster between the orogen and upper crust evolution curves (Fig. 4a), similar to ores (Makmal, Kumtor) of the MTS-E, which plot just below the orogen curve (Fig. 4a). Mineral deposits of the NTS-E define a highly correlated linear trend with a slope of 0.1507 in the uranogenic diagram (Fig. 4a). In the thorogenic diagram, the deposits of the MTS-E and NTS-E plot at slightly more thorogenic values than deposits of the MTS-W, STS-W, and Chinese Altay (Fig. 4b).

Table 4 Lead isotope compositions of rocks and silicate minerals from the lithologies of Table 2

Sample	Mineral/rock	$^{206}Pb/^{204}Pb$	$^{207}Pb/^{204}Pb$	$^{208}Pb/^{204}Pb$	Provenance
Kyzylkum segment of Southern Tien Shan (STS-W)					
401700-Kf	Kf in granite	18.433	15.662	38.389	Koshrabad
401701-Kf	Kf in granite	18.501	15.676	38.446	Koshrabad
43-Kf	Kf in granite	18.582	15.660	38.372	Muruntau
44-Kf	Kf in granite	18.470	15.649	38.372	Muruntau
45-Kf	Kf in granite	18.337	15.637	38.260	Muruntau
12-L	schist	18.595	15.731	39.349	Muruntau
12-R	schist	19.715	15.780	39.637	Muruntau
14a-L	schist	19.948	15.814	40.208	Muruntau
14a-R	schist	18.672	15.715	38.711	Muruntau
401200-L	Aplitic granite	28.451	16.013	44.138	Sarytau
401200-R	Aplitic granite	19.039	15.694	38.551	Sarytau
401201-R	Granite	18.851	15.674	38.508	Sarytau
401201-L	Granite	23.873	15.946	42.287	Sarytau
Northern Tien Shan east of Talas-Farghona fault (NTS-E)					
Akkulen	Kf in syenite	18.021	15.571	38.077	Akkulen
320000-WR	Granite[f]	21.738	15.760	41.423	Aktyuz
320000[a]	Granite[f]	*21.575*	*15.760*	*n.d.*	Aktyuz
320000-L	Granite[f]	18.490	15.570	39.143	Aktyuz
320000-L-rep	Granite[f]	22.573	15.813	42.431	Aktyuz
320000-R	Granite[f]	19.456	15.629	38.661	Aktyuz
320000-R-rep	Granite[f]	19.545	15.604	38.587	Aktyuz
320001-L	Granite[f]	22.555	15.796	42.341	Aktyuz
320001-R	Granite[f]	23.746	15.848	39.555	Aktyuz
320300a-Kf	Kf in granite[f]	18.451	15.578	38.199	Boordu
320300b-Kf	Kf in granite[f]	18.487	15.599	38.244	Boordu
320300-L	Granite[f]	19.736	15.691	40.558	Boordu
320300-R	Granite[f]	18.369	15.577	38.210	Boordu
Middle Tien Shan east of Talas-Farghona fault (MTS-E)					
350004-L	Schist	18.534	15.587	38.603	Kumtor
350004-R	Schist	21.349	15.676	42.540	Kumtor
350004	Syngenetic pyrite[g]	17.987	15.548	38.477	Kumtor
Schist 1	Py in schist	18.184	15.585	38.916	Kumtor
Schist 2	Pyrite	18.021	15.572	38.326	Kumtor
Schist 2-corr[b]	Pyrite	*18.019*	*15.572*	*n.d.*	Kumtor
320100-WR	Granite	20.594	15.697	39.887	Makmal
320100[c]	Granite	*20.543*	*15.697*	*n.d.*	Makmal
320100-L	Granite	24.516	15.905	42.535	Makmal
320100-R	Granite	18.020	15.559	38.103	Makmal
320101-WR	Granite	18.723	15.598	39.378	Makmal
320101[d]	Granite	*18.722*	*15.597*	*n.d.*	Makmal
320101-L	Granite	19.787	15.669	40.760	Makmal
320101-R	Granite	17.951	15.542	38.062	Makmal
Kokshaal segment of Southern Tien Shan (STS-E)					
206201	Kf in granite	18.253	15.636	38.429	Uchkoshkon
206802	Kf in granite	18.116	15.609	38.314	Uchkoshkon
208901	Kf in granite	18.366	15.690	38.675	Djangart
209103	Kf in granite	18.287	15.681	38.567	Djangart
215604	Kf in granite	18.243	15.666	38.487	Akshiyrak

Table 4 (continued)

Sample	Mineral/rock	$^{206}Pb/^{204}Pb$	$^{207}Pb/^{204}Pb$	$^{208}Pb/^{204}Pb$	Provenance
220203	Kf in granite	18.234	15.609	38.424	Mudryum
221802	Kf in granite	18.168	15.593	38.325	Kokkiya
209001	Pyrite in alkaline rock	18.402	15.687	38.648	Sarysay
209001[e]	Pyrite in alkaline rock	*18.401*	*15.687*	*n.d.*	Sarysay
Altay					
xj9-Kf	Kf in granite	18.287	15.543	38.111	Shangkelan

Values corrected for U decay at the age of the intrusion (Table 2) are reported in italics

n.d. not determined, *rep* repeated, *WR* whole rock, *L* leachate, *R* residue, *Kf* K-feldspar (for details on the analytical procedures, see text)

[a] Corrected for time-integrated decay of U for an age of 280 Ma, Pb=15 ppm, and U=0.77 ppm (measured by isotope dilution)

[b] Corrected for time-integrated decay of U for an age of 280 Ma, Pb=550 ppm, and U=0.32 ppm (measured by isotope dilution)

[c] Corrected for time-integrated decay of U for an age of 280 Ma, Pb=25 ppm, and U=0.43 ppm (measured by isotope dilution)

[d] Corrected for time-integrated decay of U for an age of 280 Ma, Pb=36 ppm, and U=0.01 ppm (measured by isotope dilution)

[e] Corrected for time-integrated decay of U for an age of 280 Ma, Pb=325 ppm, and U=0.89 ppm (measured by isotope dilution)

[f] Altered rock

[g] Pb=304 ppm

Ore deposits of the Chinese Altay are characterized by low $^{207}Pb/^{204}Pb$ values, ranging between the mantle and orogen curves of Zartman and Doe (1981), and by a narrow range of $^{206}Pb/^{204}Pb$ values (Fig. 4).

Discussion

We discuss the Pb isotope data from three points of view: (1) the regional and large-scale (terrestrial reservoir) sources of lead in the magmatic rocks and ore deposits, (2) the possible existence of a preferential metal reservoir for the giant Au deposits of the Southern Altaids, and (3) the Pb isotope implications concerning the basement composition of the investigated transect.

Lead sources in crustal rocks and ore deposits

Despite different origins and ages, ore minerals and magmatic rocks have consistent Pb isotope signatures within each terrane (Fig. 4) suggesting that terrane lithologies had a dominant control on the isotopic compositions of both magmatic and hydrothermal activities.

Magmatic rocks, metasediments, and orogenic Au deposits of the STS-W have altogether ^{207}Pb-enriched signatures (Fig. 4a), suggesting derivation from an old upper continental crust characterized by elevated μ values (μ~10.3 following the model of Stacey and Kramers 1975). Signatures of the STS-W ore deposits overlap only in part those of the associated Kyzylkum Segment intrusive rocks and extend towards higher $^{207}Pb/^{204}Pb$ values typical of the Besopan schists (Fig. 4), suggesting that ore lead is a mixture between these two reservoirs. The variable Pb signatures within single deposits (e.g., Guzhumsay, Sarmich) suggest a lack of homogenization of the fluids at the deposit scale.

The signatures of deposits of the MTS-W, formed in a continental arc environment, reflect derivation of lead from a homogeneous reservoir, most likely represented by the continental arc magmas. Indeed, the signatures of these deposits, plotting just above the orogen curve of Zartman and Doe (1981), are typical of the continental arc environment where mantle-derived magmas interact with and become contaminated by ^{207}Pb-rich continental crust rocks. This interpretation is consistent with $^{87}Sr/^{86}Sr_i$ data (0.7061 to 0.7075; Solomovich 1997) on magmatic rocks of the Beltau-Kurama arc that indicate mixed mantle and crustal sources typical of a continental arc setting.

Common lead isotope compositions of the ore deposits of the NTS-E plot along a highly correlated trend (R=0.9916) in the uranogenic plot (Fig. 4a) with a slope of 0.1507, that intersects the Stacey and Kramers (1975) growth curve at 341 Ma. This trend represents an anomalous lead line, which requires mixing between a Pb source that separated from the Stacey and Kramers reservoir at about 341 Ma (we do not attach much value to this age that roughly represents the Paleozoic mineralization time of the deposits of the NTS-E; Table 1) and radiogenic Pb that accumulated in rocks since 1.43 or 2.18 Ga using the equations of the instantaneous and continuous models, respectively (Kanasewich 1968). In other words, the lead isotope compositions of the NTS-E ores derive from mixing of a common lead source, separated from the Stacey and Kramers reservoir during the Paleozoic, with radiogenic lead derived from a Proterozoic basement.

The compositions of deposits of the MTS-E (Makmal and Kumtor) overlap the least radiogenic part of the fields of both the associated intrusions and of the Jetym schists (Fig. 4). The coincidence between isotopic compositions of the metasedimentary rocks, magmatic rocks, and ores suggests that both magmatism and hydrothermal fluids have essentially recycled the basement material in this terrane. The ^{207}Pb-poorer signatures of the Vendian Jetym schists (MTS-E), compared to the Cambrian Besopan

schists (STS-W), point to different primary sources of the sediments that host the orogenic-Au deposits in the MTS-E and STS-W terranes (Fig. 4a).

The Chinese Altay ore deposits have consistently low $^{207}Pb/^{204}Pb$ values and no thorogenic lead enrichment, suggesting a dominant mantle contribution (Fig. 4a). The ore deposits with the lowest $^{207}Pb/^{204}Pb$ values (Cu–Ni magmatic deposit of Kalatonge and Cu-VHMS deposit of Ashele) are associated with mafic or bimodal rocks of various tectonic settings (post-collisional extension, Kalatonge; near-continent rift or oceanic island arc, Ashele) and plot across the mantle evolution curve suggesting a 100% mantle origin for their lead. The Zn–Pb VHMS deposit of Keketale, the four samples from the orogenic-Au deposit of Saidu, the Shangkelan pyrite-rich granite, and the Au–W deposit of Manka plot within a narrow field characterized by higher $^{207}Pb/^{204}Pb$ values that suggest some crustal contamination.

The steep trend defined by Pb isotope signatures of the magmatic rocks of the STS-E in the uranogenic plot indicates mixing between upper crust and a less radiogenic Pb source (Figs. 3 and 4). The thorogenic lead enrichment of these rocks (Fig. 4) indicates a significant contribution from old metamorphosed rocks with lower crust-type isotopic compositions.

Gold sources in deposits of the Southern Altaids

The Southern Altaids contain numerous world-class Au-bearing deposits of various genetic affiliations (including porphyry, skarn, and epithermal and orogenic gold types), among which we have investigated Taldybulak Levoberezhny (3.5 Moz Au), Muruntau (175 Moz Au), Daugyztau (6 Moz Au), Amantaitau (4 Moz Au), Zarmitan (11.3 Moz Au), Makmal (2 Moz Au), Kumtor (19 Moz Au), Kalmakyr (93 Moz Au), and Kochbulak (4.3 Moz Au), only to mention the largest ones (see Yakubchuk et al. 2002). A question that might arise is whether an enriched metal reservoir could be a first-order factor responsible for the gold enrichment in the Altaids orogen. Lead isotopes have been widely used in the past as tracers of metal sources in mineralization because it is considered that lead and metals like Cu, Zn, Au, and Ag behave similarly in hydrothermal solutions. However, because the distribution of lead is not necessarily coupled with that of chalcophile metals like Cu and Au in different lithologies, hydro-thermal leaching of lithologies with strongly different concentrations of Pb, Cu, and Au may result in lead isotope compositions of the precipitated ore minerals that are biased in favor of the Pb-rich lithology, which is not necessarily also the Cu- and Au-rich one (see Chiaradia et al. 2004). This poses a limit to the usefulness of Pb isotopes as tracers of the sources of other metals in ore deposits.

The large isotopic differences of ore minerals from the gold deposits of the Southern Altaids show that there is apparently no preferential reservoir of lead, and that lead was derived from the terrane basement hosting the mineral deposits, but they do not exclude the possibility of a (Pb-poor) preferential gold reservoir that has been masked by mixing with a Pb-rich (gold-poor) reservoir during the ore-forming processes.

Spatial variations of lead isotope compositions in the Southern Altaids crust

We discuss the variations of Pb isotope compositions of ore deposits and magmatic rocks through the "uranogenic" and "thorogenic components" (Fig. 5) because these components measure the shift of each sample with respect to the orogen curve of Zartman and Doe (1981) in the uranogenic and thorogenic plots. As such, these components provide a visualization of the contributions from the mantle, upper crust, and lower crust reservoirs that is not biased by growth of radiogenic lead due to age differences. Upper crust contributions are well-discriminated from lower crust and mantle contributions by the uranogenic Pb component, whereas the lower crust can be discriminated from the mantle by the thorogenic Pb component (Fig. 5a,b).

Figure 5a shows a systematic decrease of the uranogenic Pb component from SW to NE, which suggests an eastward increasing mantle or lower crust lead contribution. Combining the information of the uranogenic and thorogenic components (Fig. 5), we infer that the uranogenic component decrease in the terranes of the central part of our transect (MTS-W, NTS-E, MTS-E, and STS-E) is due to a significant lower crustal lead contribution (with the exception of the Boordu-Taldybulak Levoberezhny ores and magmatic rocks that display upper crust- and mantle-derived lead contributions, respectively), whereas the concomitant low uranogenic and thorogenic Pb in the Chinese Altay can only be related to a significant mantle lead input (Fig. 5a,b). The westernmost terrane (STS-W) of our transect is characterized overall by low thorogenic and high uranogenic Pb due to upper crust-type lead. Only the ore cluster of Muruntau, Amantaitau, and Daugyztau has significantly higher thorogenic Pb (Fig. 5b), suggesting that ore solutions have probably leached also lower crust-type rocks characterized also by high ω ($^{232}Th/^{204}Pb$) values in this part of the terrane.

In summary, our data indicate a heterogeneous crust in the Southern Altaids with a dominantly juvenile crust northeast of 80° E and a dominantly continental crust, including both upper and lower crust-type rocks, southwest of 80° E in the investigated transect. The impact of lower crust-type rocks on the isotopic compositions of magmas and ores is widespread in the Middle and Northern Tien Shan (MTS-W, MTS-E, NTS-E) and in the Kokshaal Segment of the Southern Tien Shan (STS-E), whereas it is only local in the Kyzylkum Segment of the Southern Tien Shan (STS-W). Proterozoic to Archean rocks are known to occur in the Middle and Northern Tien Shan as well as in the Kokshaal Segment of the Southern Tien Shan, thrusted over the Tarim basement (e.g., Jenchuraeva 2001; Kiselev and Maksumova 2001), thus explaining the thorogenic Pb-rich signatures of rocks and ores in these terranes. In the Boordu-Taldybulak Levoberezhny district, magmas dis-

Fig. 5 Uranogenic Pb (**a**) and thorogenic Pb (**b**) components vs longitude diagrams for the mineral deposits and magmatic rocks analyzed. The uranogenic and thorogenic components represent the difference between $^{207}Pb/^{204}Pb$ and $^{208}Pb/^{204}Pb$ values, respectively, of the sample and the orogen curve of Zartman and Doe (1981) calculated at the $^{206}Pb/^{204}Pb$ value of the sample

play an upper crust contribution compared to all other investigated areas within the Middle and Northern Tien Shan, but the reason of this is not clear presently.

In contrast, in the Kyzylkum Segment of the Southern Tien Shan there is no evidence for a high-grade Paleo-Proterozoic and Archaean basement, which explains the dominant upper crustal signature (without a lower crust-type component) in most of the ores and all the magmatic rocks of the STS-W. This upper crustal signature probably indicates that the basement in this region is mainly composed of low-grade metamorphosed Neo-Proterozoic and Lower Paleozoic rocks similar to the schists of the Besopan Group (Brookfield 2000). The only exception is represented by the cluster of orogenic gold deposits of Muruntau, Amantaitau, and Daugyztau whose thorogenic Pb component suggests leaching of old metamorphic rocks,

perhaps representing a hidden Precambrian basement sliver.

In the Chinese Altay, the dominantly juvenile lead component, with some contribution from the continental crust, of magmatic rocks and associated ores is consistent with the ε_{Nd} values (−5 to +5) of granites of Xinjiang Altay (Jahn et al. 2000) and reflects the variable interaction of mantle-derived magmas with slivers of Precambrian continental crust in this part of the orogen.

Conclusions

In this study, we have presented the first extensive data set of lead isotope compositions of ores and crustal rocks of the Southern Altaids. Our data indicate that Pb isotope

compositions of ore deposits and crustal rocks of the Tien Shan and Chinese Altay are terrane-dependent and thus support the fact that the Altaid orogen is a collage of different blocks. The terranes investigated are characterized by a systematic decrease of the uranogenic Pb component from southwest to northeast, which can be explained by an increasing contribution of the lower crust in the Middle and Northern Tien Shan (MTS-W, MTS-E, NTS-E) and in the Kokshaal Segment of the Southern Tien Shan (STS-E), and of a MORB-type mantle in the Chinese Altay. This is in agreement with geodynamic reconstructions that interpret the Altay as the result of accretion of subduction complexes, island arcs, remnants of oceanic floor, and minor Precambrian crustal slivers and with the widespread occurrence of Proterozoic and Archaean blocks in the Middle-Northern Tien Shan and in the Kokshaal Segment thrusted over the Precambrian Tarim basement.

The major orogenic, epithermal, and intrusion-related gold deposits, situated in various terranes of the studied transect, are characterized by different Pb isotopic compositions. Whereas this apparently excludes the occurrence of a preferential reservoir supplying the huge amounts of gold in the deposits of the Southern Altaids, it cannot be ruled out that such a reservoir has been masked in the lead isotope systematics by mixing processes with Pb-richer (Au-poor) reservoirs during the mineralizing events.

References

Abeleira A, Ansdell KM, Heaman L (2000) U–Pb and Nd isotope constraints on the evolution of the Tien Shan, Kumtor region, Kyrgyzstan. In: Geological Society of America Summit 2000, Reno, Nevada (Abstracts with Programs)

Allen MB, Windley BF, Zhang C (1992) Paleozoic collisional tectonics and magmatism of the Chinese Tien Shan, Central Asia. Tectonophysics 220:89–115

Allen MB, Sengör AMC, Natal'in BA (1995) Junggar, Turfan and Alakol basins as late Permian to Early Triassic extensional structures in a sinistral shear zone in the Altaid orogenic collage, Central Asia. J Geol Soc (Lond) 152:327–338

Ansdell KM, Abeleira A, Ivanov S (1999) Structural evolution and vein paragenesis at the Kumtor gold deposit, Kyrgyzstan. In: Stanley CJ et al (eds) Mineral deposits: processes to processing. Balkema, Rotterdam, pp 1375–1378

Askerova J (1996) Fluid regime of metamorphism of Lower-Paleozoic series and fluid inclusions in quartz veins of the Sarmich gold deposit (S. Nuratau, Western Uzbekistan). Proceedings, PACROFI VI, Madison W, electronic program

Biske G, Yu S, Shilov G (1998) Structure of the northern margin of Tarim massif (Eastern Kokshaal area, Tien Shan). Geotectonics 32:51–59 (English translation by MAIK Nauka/Interperiodica)

Bortnikov NS, Prokof'ev VY, Razdolina NV (1996) Origin of the Zharmitan gold-quartz deposit (Uzbekistan). Geol Ore Depos 38:208–226

Brookfield ME (2000) Geological development and Phanerozoic crustal accretion in the western segment of the southern Tien Shan (Kyrgyzstan, Uzbekistan and Tajikistan). Tectonophysics 328:1–14

Carignan J, Gariépy C, Machado N, Rive M (1993) Pb isotopic geochemistry of granitoids and gneisses from the late Archean Pontiac and Abitibi Subprovinces of Canada. Chem Geol 106:299–316

Carroll AR, Graham SA, Chang EZ, McKnight C (2001) Sinian through Permian tectonostratigraphic evolution of the north-western Tarim basin, China. In: Hendrix MS, Davis GA (eds) Paleozoic and Mesosoic tectonic evolution of central Asia: from continental assembly to intracontinental deformation. Mem Geol Soc Amer 194:47–69

Chen C, Lu H, Jia D, Cai D, Wu S (1999) Closing history of the southern Tianshan oceanic basin, western China: an oblique collisional orogeny. Tectonophysics 302:23–40

Chen J, Zhou T, Xie Z, Zhang X, Guo X (2000a) Formation of positive ε_{Nd}(T) granitoids from the Alataw Mountains, Xinjiang, China, by mixing and fractional crystallization: implication for Phaneoroic crustal growth. Tectonophysics 328:53–67

Chen F, Li H, Wang D, Cai H, Chen W (2000b) New chronological evidence for Yanshanian diagenetic mineralization in China's Altay orogenic belt. Chin Sci Bull 45:108–113

Chiaradia M (2003) The evolution of tungsten sources in crustal mineralization from Archean to Tertiary inferred from lead isotopes. Econ Geol 98:1039–1045

Chiaradia M, Fontboté L (2003) Separate lead isotope analyses of leachate and residue rock fractions: implications for metal source tracing. Miner Depos 38:185–195

Chiaradia M, Fontboté L, Paladines A (2004) Metal sources in mineral deposits and crustal rocks of Ecuador (1° N–4° S): a lead isotope synthesis. Econ Geol 99:1085–1106

Curti E (1987) Lead and oxygen isotope evidence for the origin of the Monte Rosa gold lode deposits (Western Alps, Italy): a comparison with Archean lode deposits. Econ Geol 82:2115–2140

Drew LJ, Berger BR, Kurbanov NK (1996) Geology and structural evolution of the Muruntau gold deposit, Kyzylkum desert, Uzbekistan. Ore Geol Rev 11:175–196

Feng Y, Coleman RG, Tilton G, Xiao X (1989) Tectonic evolution of the west Junggar region, Xinjiang, China. Tectonics 8:729–752

Goldfarb R, Mao J, Hart C, Wang D, Anderson E, Wang Z (2003) Tectonic and metallogenic evolution of the Altay Shan, Northern Xinjiang Uygur Autonomous region, Northwestern China. In: Mao J, Goldfarb R, Seltmann R, Wang D, Xiao W, Hart C (eds) Tectonic evolution and metallogeny of the Chinese Altay and Tianshan. International Association on the Genesis of Ore Deposits (IAGOD), London, Guidebook Series 10, pp 17–30

Gulson BL (1977) Lead isotope results of acid leaching experiments on acid volcanics and black shales in an ore environment. Geochem J 11:239–245

Han BF, Wang SG, Jahn BM, Hong DW, Kagami H, Sun YL (1997) Depleted-mantle source for the Ulungur River A-type granites from North Xinjiang, China—Geochemistry and Nd-Sr isotopic evidence, and implications for Phanerozoic crustal growth. Chem Geol 138:135–159

Hart C, Wang Y, Goldfarb R, Begg G, Mao J, Dong L (2003) Axi and associated epithermal gold deposits in the western Tianshan, Xinjiang, P. R. China. In: Mao J, Goldfarb R, Seltmann R, Wang D, Xiao W, Hart C (eds) Tectonic evolution and metallogeny of the Chinese Altay and Tianshan. International Association on the Genesis of Ore Deposits (IAGOD), London. Guidebook Series 10, pp 209–226

Heinhorst J, Lehmann B, Ermolov P, Serykh V, Zhurutin S (2000) Paleozoic crustal growth and metallogeny of Central Asia: evidence from magmatic-hydrothermal ore systems of Central Kazakhstan. Tectonophysics 328:69–87

Hong D, Wang S, Xie X, Zhang J, Wang T (2003) Granitoids and related metallogeny of the Central Asian Orogenic Belt. In: Mao J, Goldfarb R, Seltmann R, Wang D, Xiao W, Hart C (eds) Tectonic evolution and metallogeny of the Chinese Altay and Tianshan. International Association on the Genesis of Ore Deposits (IAGOD), London. Guidebook Series 10, London, pp 75-106

Jahn BM, Wu F, Chen B (2000) Massive granitoid generation in Central Asia: Nd isotope evidence and implication for continental growth in the Phaneorozoic. Episodes 23:82–92

Jenchuraeva RJ (1997) Tectonic setting of porphyry-type mineralization and hydrothermal alteration in Paleozoic arcs and active continental margins, Kyrgyz Range. Miner Depos 32:434–440

Jenchuraeva RJ (2001) Paleozoic geodynamics, magmatism, and metallogeny of the Tien Shan. In: Seltmann R, Jenchuraeva R (eds) Paleozoic geodynamics and gold deposits in the Kyrgyz Tien Shan. IGCP-373 Excursion Guidebook, International Association on the Genesis of Ore Deposits (IAGOD), London, pp 29–70

Jenchuraeva RJ, Nikonorov VV, Litvinov P (2001a) The Kumtor gold deposit. In: Seltmann R, Jenchuraeva R (eds) Paleozoic geodynamics and gold deposits in the Kyrgyz Tien Shan. IGCP-373 excursion guidebook. International Association on the Genesis of Ore Deposits (IAGOD), London, pp 139–152

Jenchuraeva RJ, Pak NT, Usmanov IA (2001b) The Makmal gold deposit. In: Seltmann R, Jenchuraeva R (eds) Paleozoic geodynamics and gold deposits in the Kyrgyz Tien Shan. IGCP-373 excursion guidebook. International Association on the Genesis of Ore Deposits (IAGOD), London, pp 82–96

Jun G, Maosong L, Xuchang X, Yaoqing T, Guoqi H (1998) Paleozoic tectonic evolution of the Tienshan Orogen, northwestern China. Tectonophysics 287:213–231

Kanasewich ER (1968) The interpretation of lead isotopes and their geological significance. In: Hamilton EI, Farquhar RM (eds) Radiometric dating for geologists. Wiley-Interscience, New York, pp 147–223

Kempe U, Seltmann R, Graupner T, Wall VJ, Matukov D, Sergeev S (2004) SHRIMP U-Pb zircon dating of hercynian granite magmatism in the Muruntau gold district (Uzbekistan). In: Khanchuk AI, Gonevchuk GA, Mitrokhin AN, Simanenko LF, Cook NJ, Seltmann R (eds) Metallogeny of the Pacific Northwest: tectonics, magmatism, and metallogeny of active continental margins. Proceedings of the interim IAGOD conference, Vladivostok, Russia, 1–20 Sept 2004, pp 210–213

Kiselev VV, Maksumova RA (2001) Geology of the Northern and Middle Tien Shan: principal outlines. In: Seltmann R, Jenchuraeva R (eds) Paleozoic geodynamics and gold deposits in the Kyrgyz Tien Shan. IGCP-373 excursion guidebook. International Association on the Genesis of Ore Deposits (IAGOD), London, pp 21–28

Konopelko D, Biske G, Belyatsky B, Eklund O, Seltmann R (2003a) Hercynian post-collisional magmatism of the SE Tien Shan, Kyrgyzstan: timing and metallogenic potential. In: Processes and Metallogeny of Chinese Altay (Altai) and Tianshan. Proceedings of the international field symposium in Urumqi, Xinjiang, China, 9–21 Aug 2003, pp 10–15

Konopelko D, Mao J, Du A, Piatkov A, Biske G, Seltmann R (2003b) Re-Os age of molybdenite from the Sarytau tungsten deposit and timing of Hercynian events in the Bukantau mountains, central Kyzylkum, Uzbekistan. In: Akhmedov NA (ed) Problems of ore deposits and maximizing the prospecting efficiency. Proceedings of International Scientific-Technical Conference, Tashkent, pp 379–380

Kostitsyn YA (1996) Rb–Sr isotopic study of the Muruntau deposit: Magmatism, metamorphism, and mineralization. Geochem Int 34:1009–1023

Laurent-Charvet S, Charvet J, Monie P, Shu LS (2003) Late Paleozoic strike-slip shear zones in eastern central Asia (NW China): new structural and geochronological data. Tectonics 22:1009–1032

Li H, Xie C, Chang H, Cai H, Zhu J, Zhou S (1998) Study on metallogenetic chronology of nonferrous and precious metallic ore deposits in north Xinjiang China. Geological Publishing House, Beijing, pp 1–244 (in Chinese with English abstract)

Liu Y, Zhu Y, Wang D (2003) Shear-zone related gold deposits of the southern Altay Mountains, northwestern China. In: Mao J, Goldfarb R, Seltmann R, Wang D, Xiao W, Hart C (eds) Tectonic evolution and metallogeny of the Chinese Altay and Tianshan. International Association on the Genesis of Ore Deposits (IAGOD), London, Guidebook Series 10, pp 201–208

Macfarlane AW, Petersen U (1990) Pb isotopes of the Hualgayoc area, northern Peru: implications for metal provenance and genesis of a Cordilleran polymetallic mining district. Econ Geol 85:1303–1327

Macfarlane AW, Marcet P, Le Huray AP, Petersen U (1990) Lead isotope provinces of the Central Andes inferred from ores and crustal rocks. Econ Geol 85:1857–1880

Malyukova NN (2001) The Taldybulak Levoberezhny gold deposit. In: Seltmann R, Jenchuraeva R (eds) Paleozoic geodynamics and gold deposits in the Kyrgyz Tien Shan. IGCP-373 excursion guidebook, International Association on the Genesis of Ore Deposits (IAGOD), London, pp 97–110

Mao J, Konopelko D, Seltmann R, Lehmann B, Chen W, Wang Y, Eklund O, Usubaliev T (2004) Postcollisional age of the Kumtor gold deposit and timing of Hercynian events in the Tien Shan, Kyrgyzstan. Econ Geol 99:1771–1780

Marschik R, Chiaradia M, Fontboté L (2003) Implications of Pb isotope signatures of rocks and iron oxide Cu–Au ores in the Candelaria-Punta del Cobre district, Chile. Miner Depos 38:900–912

Morelli RM, Creaser RA, Seltmann R (2004) Rhenium–osmium geochronology of arsenopyrite from the giant Muruntau Au deposit, Uzbekistan. In: Khanchuk AI, Gonevchuk GA, Mitrokhin AN, Simanenko LF, Cook NJ, Seltmann R (eds) Metallogeny of the Pacific Northwest: tectonics, magmatism, and metallogeny of active continental margins. Proceedings of the interim IAGOD conference, Vladivostok, Russia, 1–20 Sept 2004, pp 510–513

Mukhin PA, Abdullayev KA, Minayev VY, Khristov SY, Egamberdyyev SA (1989) The paleodynamics of Central Asia. Int Geol Rev 31:1073–1083

Rui Z, Goldfarb RJ, Qiu Y, Zhou T, Chen T, Pirajino F, Yun G (2002) Paleozoic-Early Mesozoic gold deposits of the Xinjiang Autonomous Region, northwestern China. Miner Depos 37:393–418

Savchuk YS, Mukhin PA, Meshcheryakova LV (1991) Late Paleozoic granitoid magmatism and Kyzylkum ore formations from a plate tectonics point of view. Geotectonics 25:326–339

Seltmann R, Shatov V, Yakubchuk A (2005) Mineral deposits database and thematic maps of Central Asia, scale 1:1,500,000. Explanatory Notes to ArcView 3.2 and MapInfo 7 GIS packages. Centre for Russian and Central Asian Mineral Studies, NHM London, p 117

Sengör AMC, Natal'in BA (1996) Turkic-type orogeny and its role in the making of the continental crust. Annu Rev Earth Planet Sci 24:263–337

Sengör AMC, Natal'in BA, Burtman VS (1993) Evolution of the Altaid tectonic collage and Paleozoic crustal growth in Eurasia. Nature 364:299–307

Solomovich LI (1997) Petrology and ore potential of monzonite–syenite association in the Tien Shan. Petrology and ore potential of igneous rock associations in the Tien Shan. Frunze Ilim, pp 102–120 (in Russian)

Stacey JS, Kramers JD (1975) Approximation of terrestrial lead isotope evolution by a two-stage model. Earth Planet Sci Lett 26:207–221

Todt W, Cliff RA, Hanser A, Hofmann AW (1996) Evaluation of a ^{202}Pb–^{205}Pb double spike for high-precision lead isotope analyses. In: Hart S and Basu A (eds) Earth processes: reading the isotopic code. AGU Monogr 95:429–437

Tosdal RM, Wooden JL, Bouse R (1999) Pb isotopes, ore deposits, and metallogenic terranes. In: Lambert DD, Ruiz J (eds) Application of radiogenic isotopes to ore deposit research and exploration. Rev Econ Geol 12:1–28

Usmanov IA (2001) The Boordu zinc–lead deposit. In: Seltmann R, Jenchuraeva R (eds) Paleozoic geodynamics and gold deposits in the Kyrgyz Tien Shan. IGCP-373 excursion guidebook, International Association on the Genesis of Ore Deposits (IAGOD), London, pp 111–114

Wang D (2003) Geology, geochemistry and geodynamics of the Ashele VHMS Cu–Zn deposit, Northwestern Xinjiang. In: Mao J, Goldfarb R, Seltmann R, Wang D, Xiao W, Hart C (eds) Tectonic evolution and metallogeny of the Chinese Altay and Tianshan. International Association on the Genesis of Ore Deposits (IAGOD), London, Guidebook series 10, pp 153–168

Wang D, Chen Y, Xu Z, Li T, Fu X (2002) Metallogenic series and metallogeny in the Altay metallogenic province. Atomic Power, Beijing, p 493 (in Chinese)

Wang J, Wang Y, Wang S, Ding R (2003a) The Koktal Pb–Zn massive sulfide deposit. In: Mao J, Goldfarb R, Seltmann R, Wang D, Xiao W, Hart C (eds) Tectonic evolution and metallogeny of the Chinese Altay and Tianshan. International Association on the Genesis of Ore Deposits (IAGOD), London, Guidebook series 10, pp 169–180

Wang Y, Wang J, Wang S, Ding R, Wang L (2003b) Geology of the Mengku iron deposit, Xinjiang, China. In: Mao J, Goldfarb R, Seltmann R, Wang D, Xiao W, Hart C (eds) Tectonic evolution and metallogeny of the Chinese Altay and Tianshan. International Association on the Genesis of Ore Deposits (IAGOD), London, Guidebook series 10, pp 181–200

Windley BF, Allen MB, Zhang C, Zhao ZY, Wang GR (1990) Paleozoic accretion and Cenozoic redeformation of the Chinese Tien Shan Range, central Asia. Geology 18:128–131

Windley BF, Kröner A, Guo J, Qu G, Li Y, Zhang C (2002) Neoproterozoic to Paleozoic geology of the Altai orogen, NW China: new zircon age data and tectonic evolution. J Geol 110:719–737

Wörner G, Moorbath S, Harmon RS (1992) Andean Cenozoic volcanic centres reflect basement isotopic domains. Geology 20:1103–1106

Xiao W, Windley BF, Badarch G, Sun S, Li J, Qin K, Wang Z (2004) Palaezoic accretionary and convergent tectonics of the southern Altaids: implications for the growth of Central Asia. J Geol Soc (Lond) 161:339–342

Yakubchuk A (2004) Architecture and mineral deposit settings of the Altaid orogenic collage: a revised model. J Asian Earth Sci 23:761–779

Yakubchuk A, Cole A, Seltmann R, Shatov V (2002) Tectonic setting, characteristics, and regional exploration criteria for gold mineralization in the Altaid orogenic collage: the Tien Shan province as a key example. Society of Economic Geology Special Publication 9:177–201

Yakubchuk A, Seltmann R, Shatov V (2003) Tectonics and metallogeny of the western part of the Altaid orogenic collage. In: Mao J, Goldfarb R, Seltmann R, Wang D, Xiao W, Hart C (eds) Tectonic evolution and metallogeny of the Chinese Altay and Tianshan. International Association on the Genesis of Ore Deposits (IAGOD), London, Guidebook series 10, pp 7–16

Yan S, Zhang Z, Wang D, Chen B, He L, Zhou G (2003) Kalatongke magmatic copper-nickel sulfide deposit. In: Mao J, Goldfarb R, Seltmann R, Wang D, Xiao W, Hart C (eds) Tectonic evolution and metallogeny of the Chinese Altay and Tianshan. International Association on the Genesis of Ore Deposits (IAGOD), London, Guidebook series 10, pp 131–152

Zartman RE (1974) Lead isotopic provinces in the Cordillera of the western United States and their geological significance. Econ Geol 69:792–805

Zartman RE, Doe BR (1981) Plumbotectonics—the model. Tectonophysics 75:135–162

Zartman RE, Haines SM (1988) The plumbotectonic model for Pb isotope systematics among major terrestrial reservoirs-a case for bi-directional transport. Geochim Cosmochim Acta 52:1327–1339

Zhou D, Graham SA, Chang EZ, Wang B, Hacker B (2001) Paleozoic tectonic amalgamation of the Chinese Tian Shan: evidence from a transect along the Dushanzi-Kuqa Highway. In: Hendrix MS, Davis GA (eds) Paleozoic and Mesosoic tectonic evolution of central Asia: from continental assembly to intracontinental deformation. Mem Geol Soc Amer 194:23–46

Zonenshain LP, Kuzmin MI, Natapov LM (1990) Geology of the USSR: a plate tectonic synthesis. AGU, Geodynamics Series Monograph 21:242